Electronic Supplementary Material (ESI) for ChemComm.

Supporting Information

MoS_2@N-doped graphitic carbon/TiO_2 photocatalysts for photocatalytic H_2 production from lignocellulosic biomass

Chi Ma,[a] Quan Cheng,[a] Ze-Xin Huang,[a] Fu-Guang Zhang,[a] Qing-Yu Liu,[a] Yong-Jun Yuan*[a]

a. College of Materials and Environmental Engineering, Hangzhou Dianzi University, Hangzhou, 310018, People's Republic of China.*E-mail: yjyuan@hdu.edu.cn.

Experimental Section

Reagent.

All chemicals and reagents were analytical grade and used as received without further purification.

Synthesis of ZIF-8.

2 mmol $Zn(NO_3)_2 \cdot 6H_2O$ and 15 mmol 1-methylimidazole were dissolved in 100 mL of methanol solution, which was then added into 100 mL of methanol solution consisting of 10 mmol 2-methylimidazole. After a rapid-mixing duration of 3 seconds, the mixture solution was aged at room temperature for 24 hours without stirring. The resulting white precipitate was separated from solution by centrifugation at 4000 rpm for 2 min and then washed by absolute ethanol, and finally dried at a vacuum drying oven at room temperature.

Synthesis of N-doped grephene carbon (NGC)

1 g ZIF-8 powder put in alumina crucible was transferred to the atmosphere furnace, which was treated by a low-temperature annealing at 120 ºC for 1 h and then a high-temperature annealing at 800 ºC for 2 h under a Ar flow, and the heating rate was 5 ºC min^{-1}. During the annealing process, the organic ligand of ZIF-8 was carbonized and converted N-doped graphitic carbon (NGC), while the zinc ions were reduced to Zn metal. The Zn metal will vaporize when the temperature is close to the boiling point of Zn metal, and residual was removed by pickling.

Synthesis of MoS_2-NGC

The ***MoS_2-NGC*** was prepared via hydrothermal method in aqueous solution

consisting of NGC, $Na_2MoO_4 \cdot 4H_2O$ and thiourea. In a typical synthesis, 100 mg NGC, 245 mg $Na_2MoO_4 \cdot 4H_2O$ and 489 mg thiourea were dispersed in 30 ml deionized water. After 10 minutes of ultrasound, the mixed solution was transferred into a 50 ml Teflon-line autoclave and then heated at 200 ^oC for 24 h. After the Teflon-line autoclave was cooled to room temperature, the black precipitate was separated from the solution via centrifugation at 5000 rpm for 5 minutes, followed by washing with absolute ethanol and dried at a vacuum drying oven at room temperature.

Synthesis of MoS_2-NGC/TiO_2 photocatalysts

The MoS_2-NGC/TiO_2 photocatalysts were prepared via hydrothermal method in aqueous solution consisting of *MoS_2-NGC*, tetrabutyl titanate ($Ti(OBu)_4$) in aqueous solution. In a typical synthesis, 1 ml $Ti(OBu)_4$ dissolved in 10 ml of absolute ethyl alcohol was added dropwise into 50 ml aqueous solution containing a certain amount of NGC. After 5 minutes of ultrasound, the mixed solution was transferred into twoTeflon-line autoclave with a volume of 50 ml and then heated at 200 ^oC for 24 h. After the Teflon-line autoclave was cooled to room temperature, the grey precipitate was separated from the solution via centrifugation at 5000 rpm for 5 minutes, followed by washing with absolute ethanol and dried at a vacuum drying oven at room temperature.

Characterization

The morphology and microstructure of materials was performed on a field emission Hitachi S-4800 scanning electron microscope (SEM, Hitachi, Japan) and JEOL JEM 2010 transmission electron microscope (TEM, JEOL, Japan). The crystalline phase

of materials was measured by a Rigaku-miniflex 6 X-ray diffractometer (Japan) equipped with Cu *K*α (λ = 0.15406 nm) radiation with a scan rate of $10^{o}\cdot min^{-1}$. XPS analysis was performed on a Thermo ESCALAB 250XI XPS system with Al Kα X-ray source, and all peaks were corrected by using the C 1s level at 284.8 eV as a strandard. The UV-vis absorbance spectra of photocatalysts was measured on a TU1901 spectrophotometer (Beijing Puyan TU1901) equipped with an integrating sphere by using $BaSO_4$ as the background. The BET surface area of TiO_2 was obtained from nitrogen adsorption-desorption isotherms measured at 77 K using a Micromeritics ASAP 2460 apparatus, the BET surface area was calculated from the adsorption data, and the pore distribution was calculated by the Barret-Joyner-Halenda method. The electrochemical measurements were performed on a CHI660E electrochemical workstation (Shanghai Chenhua Limited, China) at room temperature. Transient photocurrent and LSV measurements were performed on a standard three-electrode system composed of a Pt wire counter electrode, saturated Ag/AgCl reference electrode, and sample-coated ITO (Transient photocurrent measurements) or sample-coated glassy carbon (LSV measurements) working electrode in the presence of 0.5 M Na_2SO_4 aqueous solution as the electrolyte. The sample-coated ITO working electrode was prepared by depositing of suspension solution of photocatalyst (1 $mg\cdot ml^{-1}$) on ITO glass through spin coating method, and the sample-coated glassy carbon (LSV measurements) working electrode was prepared by coating the 0.2 $mg\cdot ml^{-1}$ photocatalyst suspension dispersed in 2% Nafion ethanol on the glassy carbon electrode. The applied electric

field voltage for transient photocurrent measurement was +0.5 V vs. RHE. For the CO_2 detection, 1 mL gas extracted from the reaction system was detected by carbon dioxide analyzer (AR8200, Smart Seneor, China). The organics were analyzed by Agilent HPLC 1260 high performance liquid chromatographic instrument. The total organic carbon (TOC) of reaction solution was measured on An Elementar Vario TOC Analyzer.

Photocatalytic H_2 production experiments

The photocatalytic H_2 production experiments were carried out in a closed gas circulation and evacuation H_2 generation system in the presence of a 300 W Xe lamp as the light resource. To prepare photocatalytic reaction solution, 50 mg photocatalyst was added to 250 ml aqueous solution containing 1 g substance in quartz reactor with a volume of 450 ml with sonication for 10 min, and then the reactor was connected to the photocatalytic reaction system. These biomass were first screened through an 80-mesh (180 μm) sieve, and the lignocellulosic biomass used for photocatalytic H_2 production was particle powder with size of less than 180 μm. Before irradiation, the reaction solution was degassed to remove the dissolved air. The temperature was maintained around room temperature by a cooling cycle water. A GC1690 online gas chromatograph with a TCD detector was used to analyze the amount of evolved H_2. The apparent quantum efficiency (AQY) of photocatalytic H_2 production performed at monochromatic light was conducted by the similar process described above expect using monochromatic light filter, and the AQY was calculated according to the following equations:

$$n_{\text{photons}} = \frac{P\lambda}{hc} \times t \qquad (1)$$

$$\text{AQY}[\%] = \frac{\text{number of reacted electrons}}{\text{number of incident photons}} \times 100$$

$$= \frac{2 \times \text{number of evolved } H_2 \text{ molecules}}{\text{number of incident photons}} \times 100 \qquad (2)$$

where *P, λ, h, c and t* is the input optical power, wavelength of the light, Planck's constant, speed of light and the illumination time, respectively.

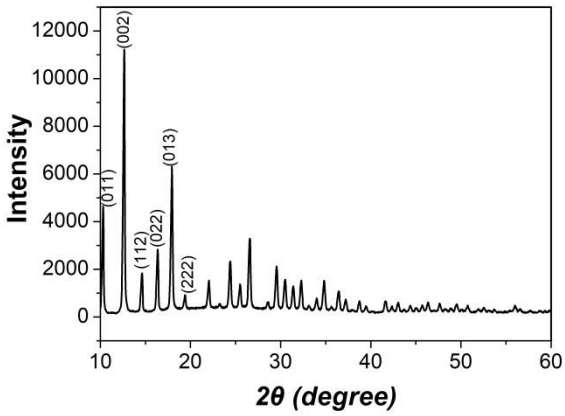

Figure S1. XRD pattern of ZIF-8.

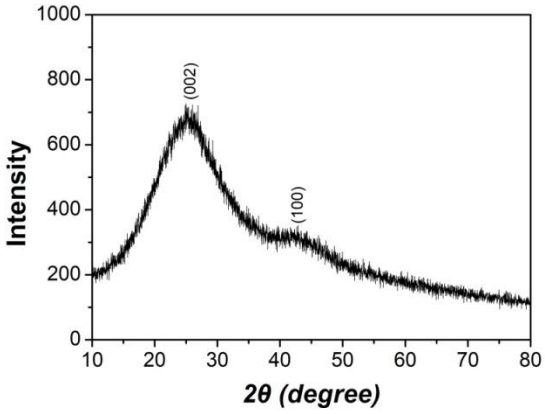

Figure S2. XRD pattern of NGC obtained via pyrolysis and acid leaching treatment of ZIF-8.

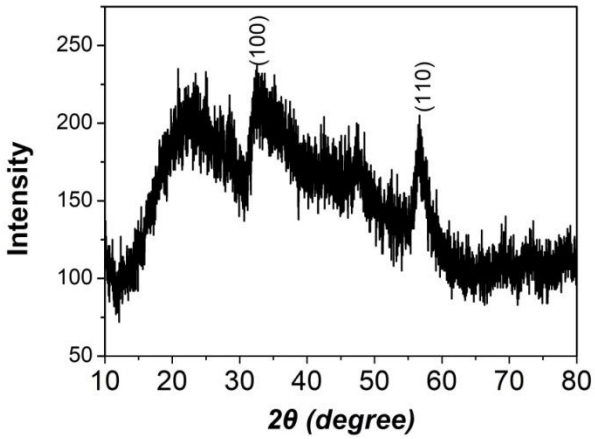

Figure S3. XRD pattern of MoS_2/NGC composite.

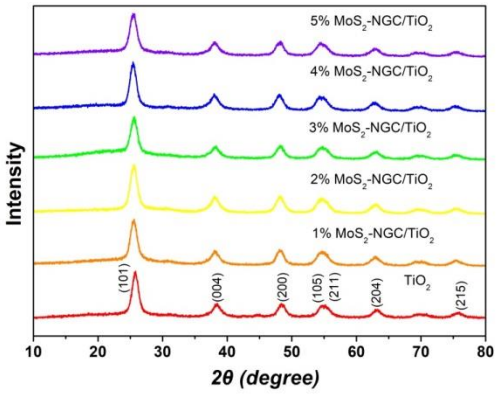

Figure S4. XRD patterns of various MoS_2-NGC/TiO_2 photocatalysts.

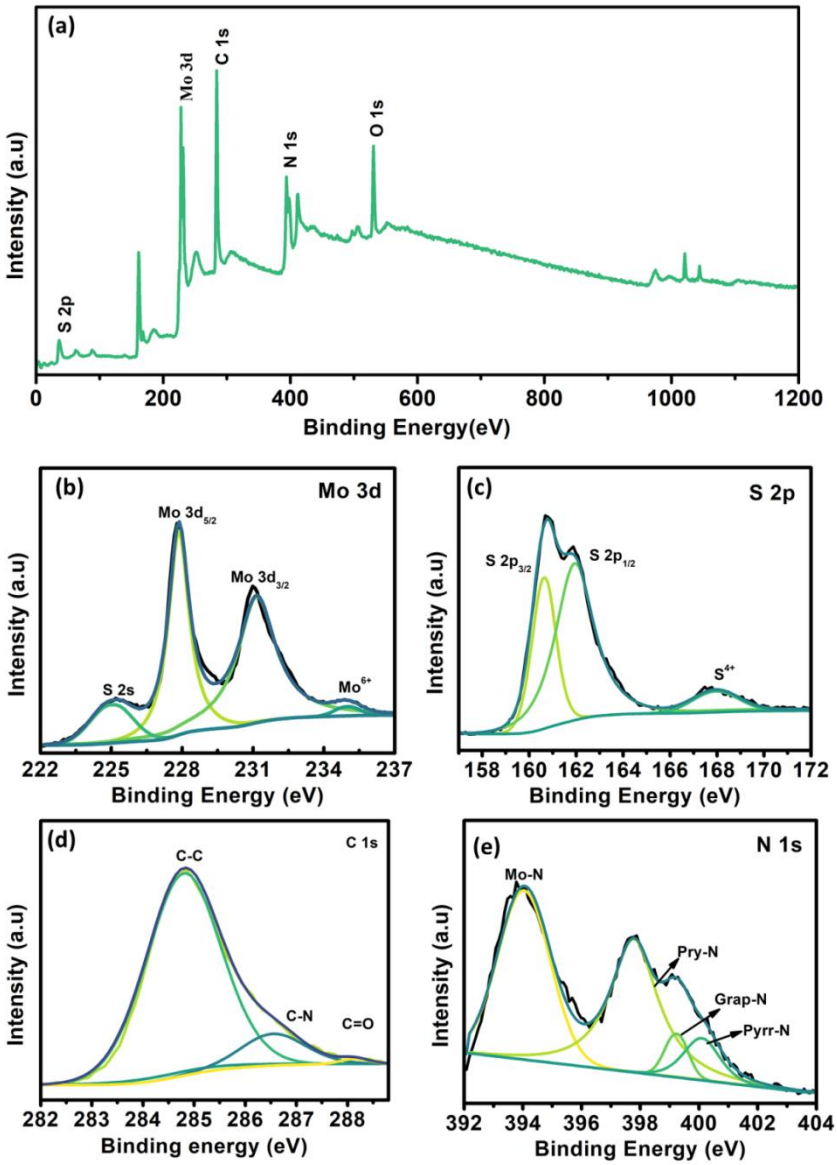

Figure S5. (a) The survey XPS spectrum for MoS_2-NGC cocatalyst. (b-e) High-resolution Mo 3d, S 2p, C 1s and N 1s of MoS_2-NGC cocatalyst.

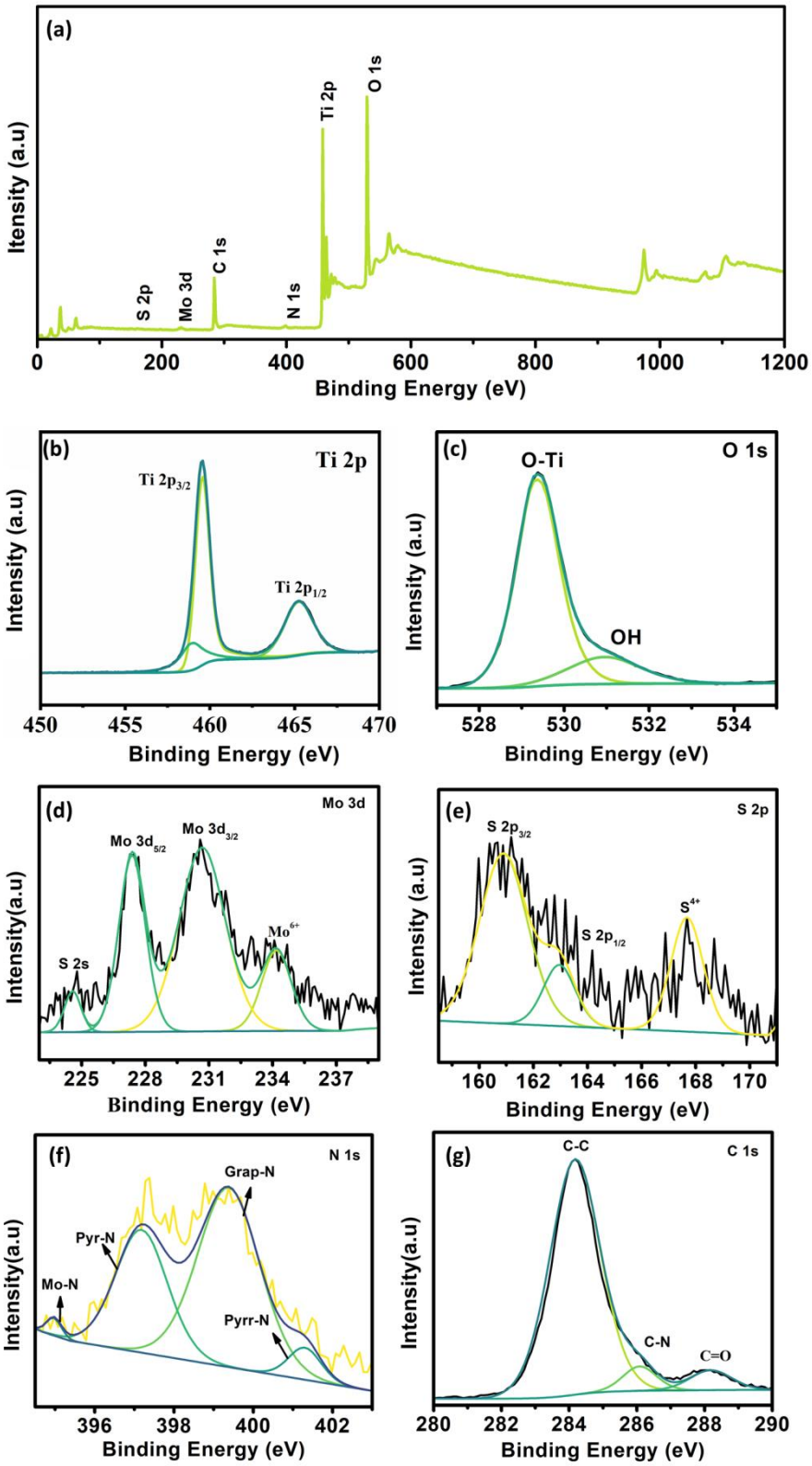

Figure S6. (a) The survey XPS spectrum for3% MoS_2-NGC/TiO_2 photocatalyst. (b-g) High- resolution Ti 2p, O 1s, Mo 3d, S 2p, N 1s and C 1s of MoS_2-NGC cocatalyst.

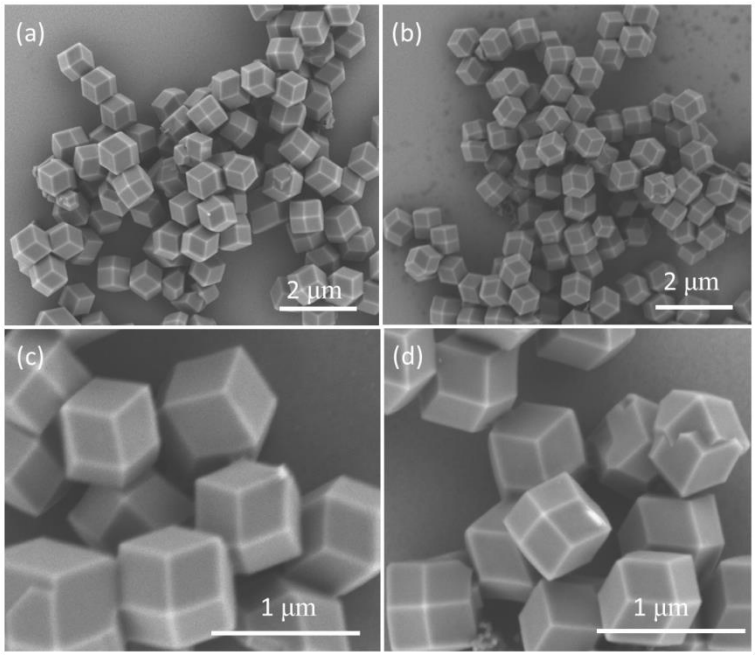

Figure S7. SEM images of ZIF-8.

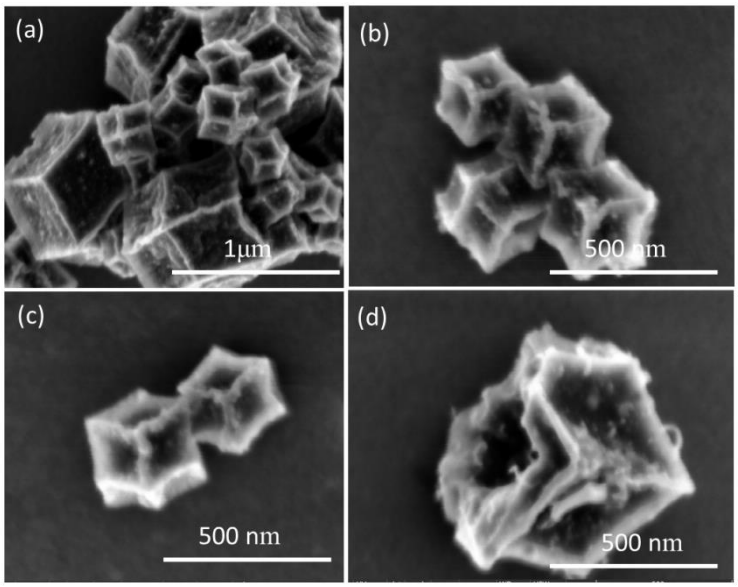

Figure S8. SEM images of NGC.

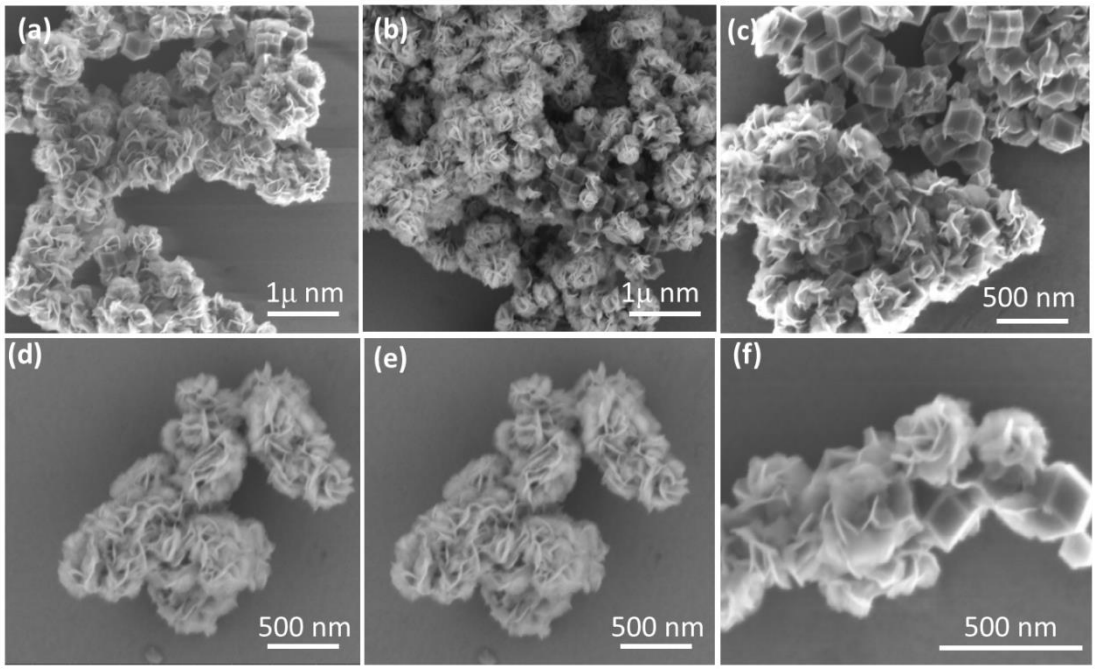

Figure S9. SEM images of MoS_2-NGC cocatalyst.

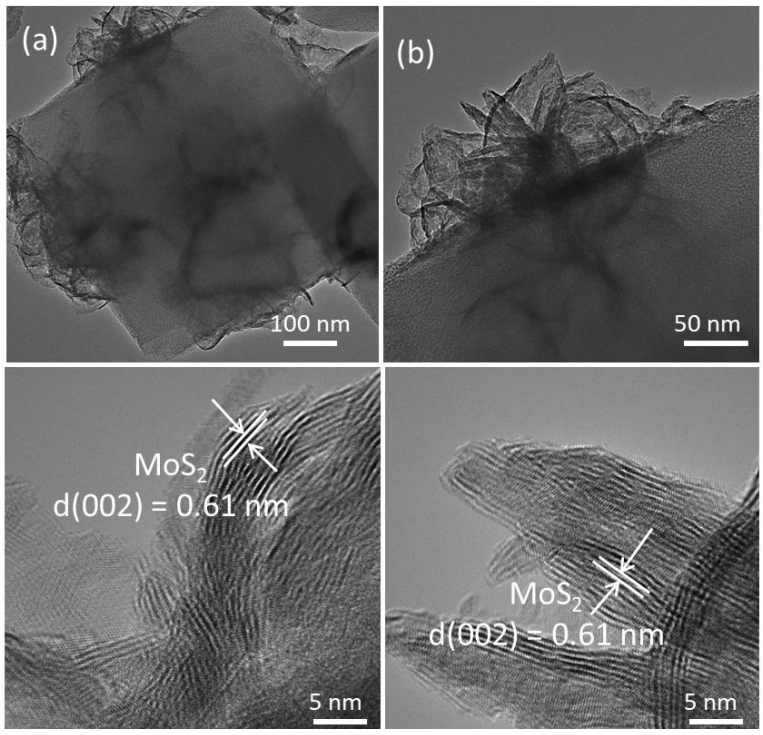

Figure S10. TEM and HRTEM images of MoS_2-NGC cocatalyst.

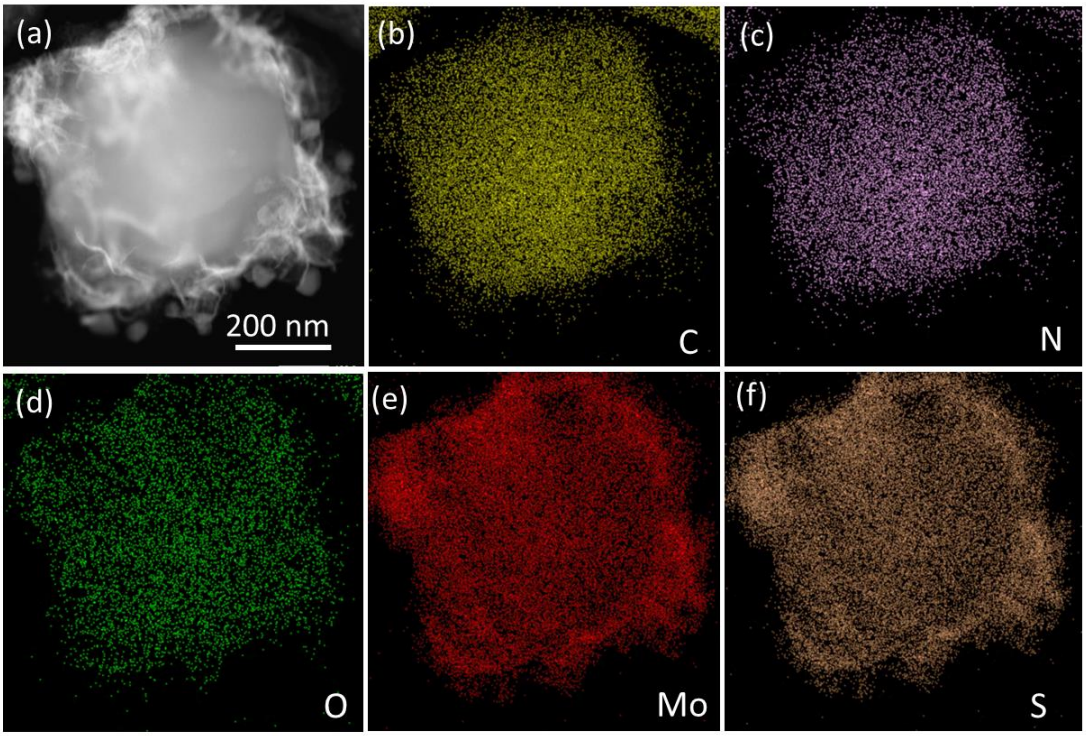

Figure S11. HAADF-STEM and elemental mapping images of MoS_2-NGC cocatalyst.

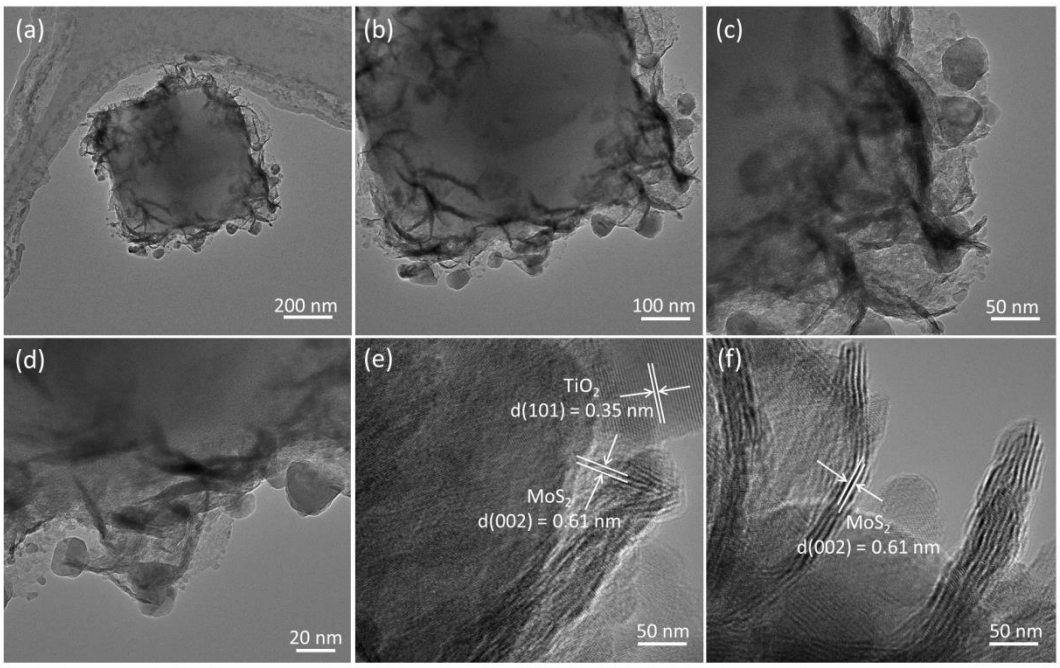

Figure S12. TEM and HRTEM images of 5% MoS_2-NGC/TiO_2 photocatalyst.

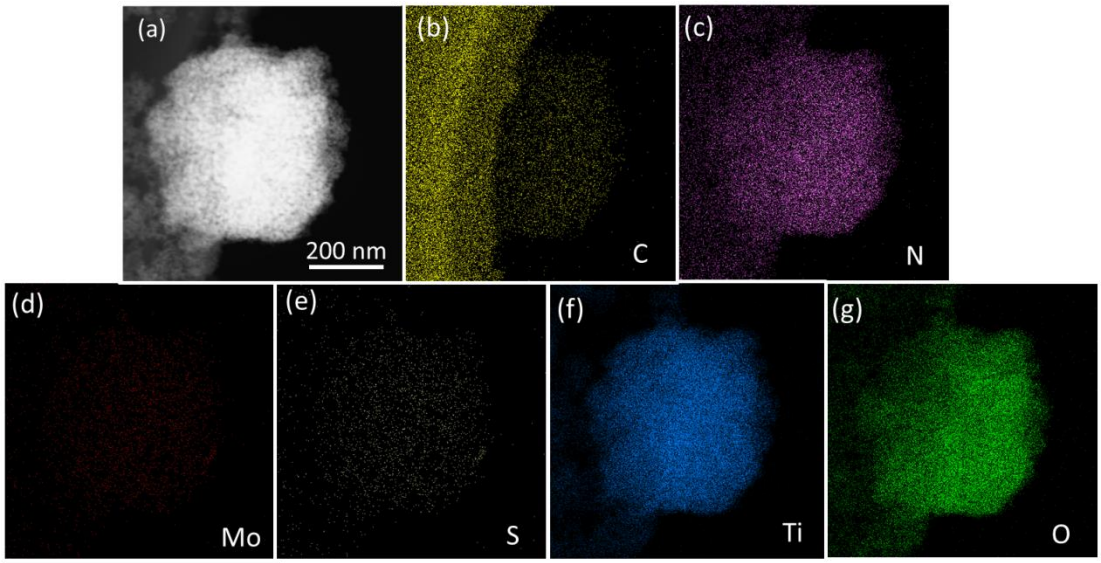

Figure S13. HAADF-STEM and elemental mapping images of 5% MoS_2-NGC/TiO_2 photocatalyst.

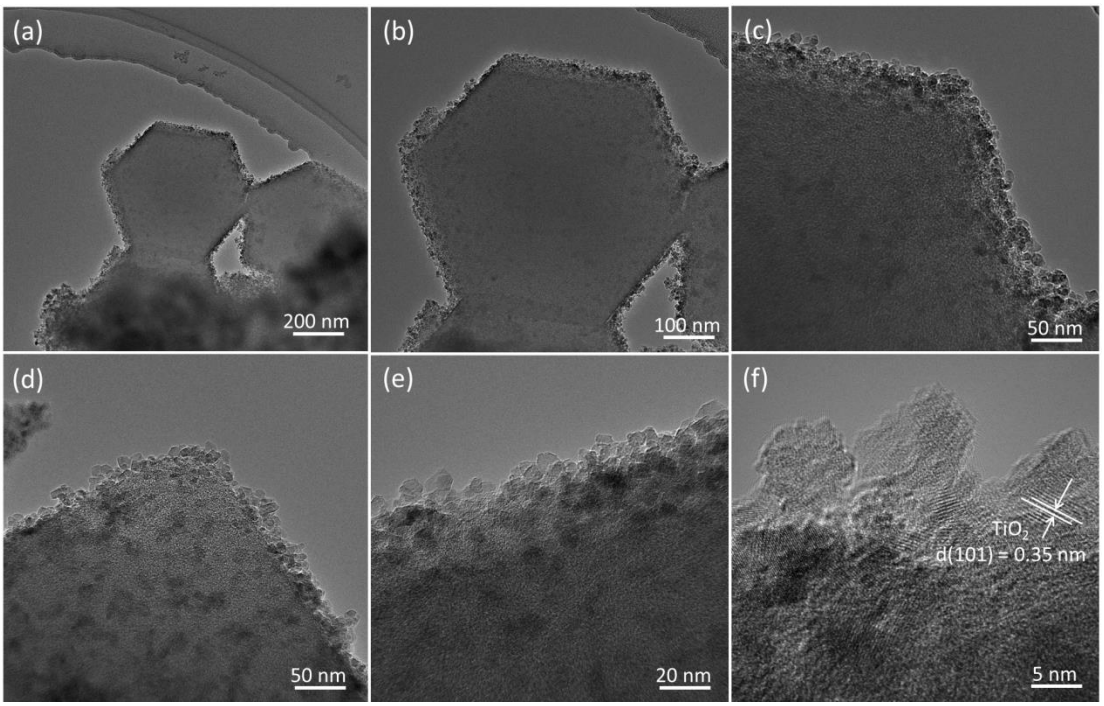

Figure S14. TEM and HRTEM images of 5% MoS_2-NGC/TiO_2 photocatalyst.

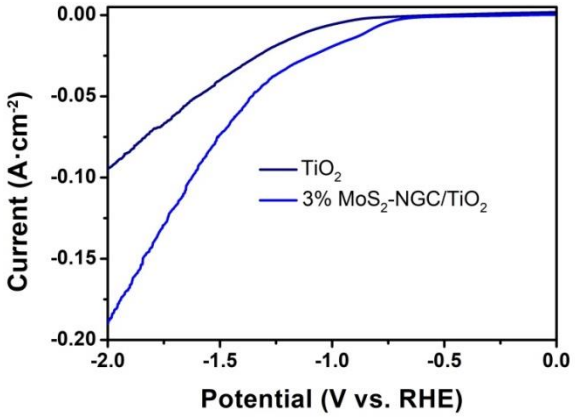

Figure S15. LSV plots of bare TiO_2 and 3% MoS_2-NGC/TiO_2 electrodes.

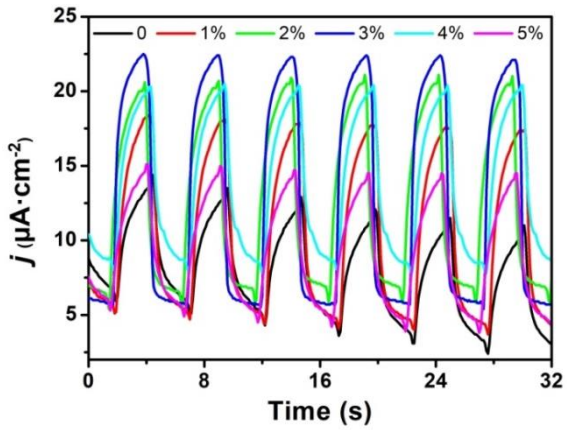

Figure S16. Photocurrent density of bare TiO_2 and various MoS_2-NGC/TiO_2 electrodes.

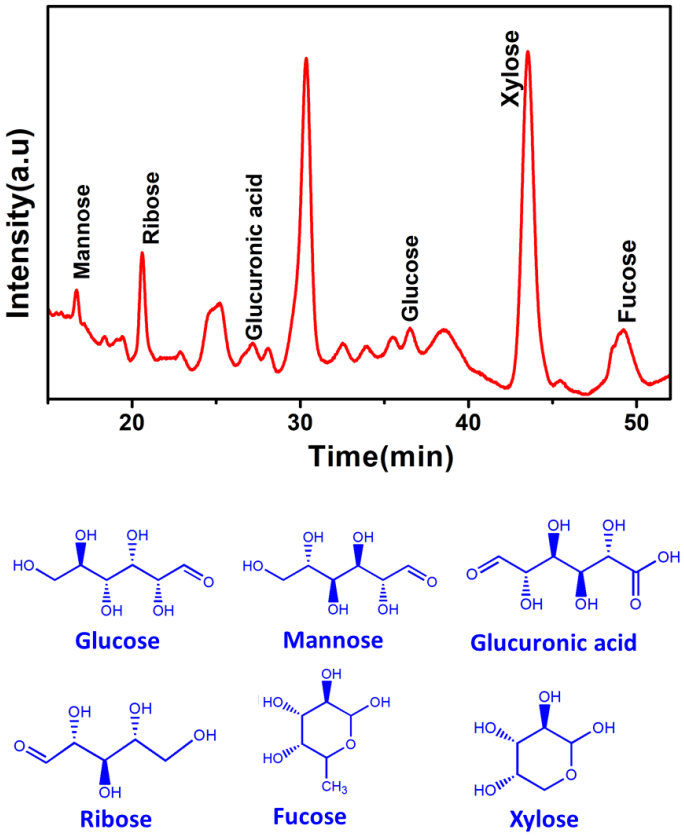

Figure S17. Liquid chromatography analysis for the sugar species as the decomposition products of α-cellulose after photocatalytic H_2 production reaction as well as their corresponding chemical structure.

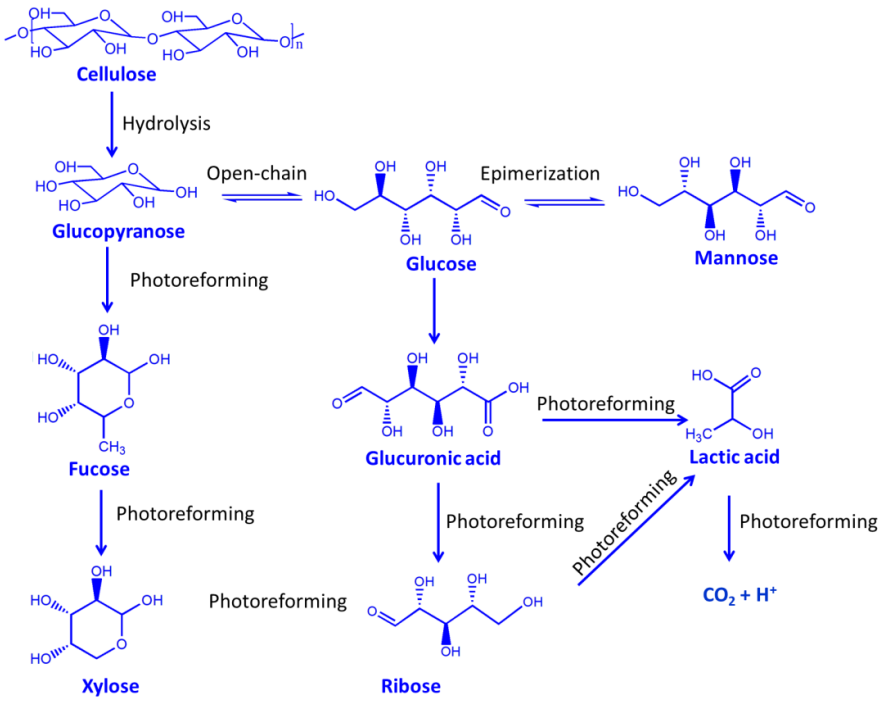

Figure S18. Proposed reaction mechanism for the decomposition of α-cellulose during photoatalytic reaction. The •OH radical with strong oxidation ability could promote the cleavage of β-1,4-glycosidic bonds of α-cellulose, resulting in the hydrolysis of α-cellulose and the formation of glucopyranose, glucose or fucose. And then, these monoses can be successively oxidized by •OH or photogenerated hole to generate galacturonic acid, lactic acid, CO_2 and other organics.

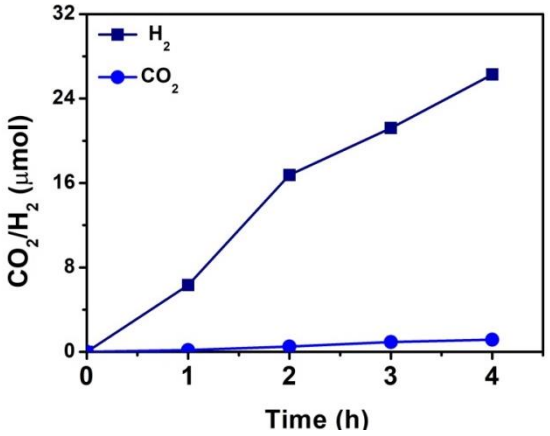

Figure S19. Time course of photocatalytic H_2 and CO_2 production over 3% MoS_2-NGC/TiO_2 photocatalyst in α-cellulose aqueous solution under 300 W Xe lamp irradiation.

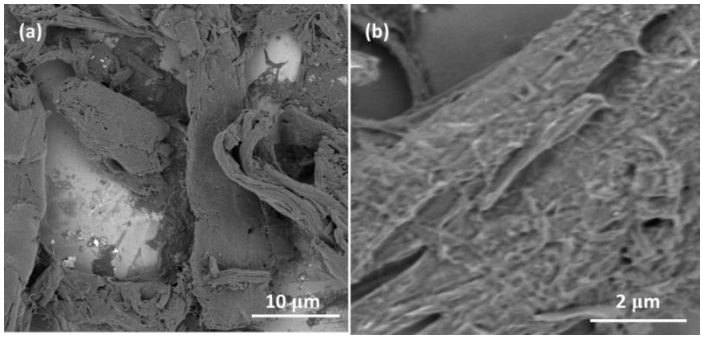

Figure S20. SEM images of fresh α-cellulose (a) and solid residue from photocatalytic H_2 production system after 8 h of irradiation and (b)

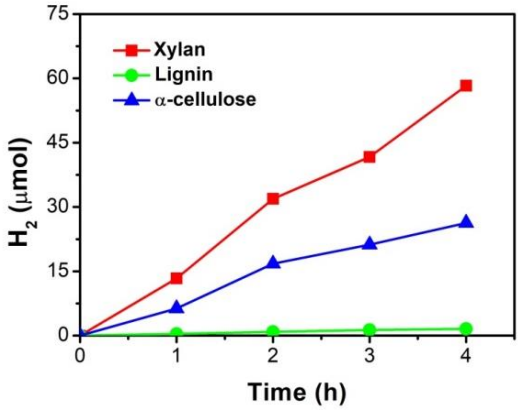

Figure S21. Time course of photocatalytic H_2 production over 3% MoS_2-NGC/TiO_2 photocatalyst in α-cellulose, hemicelluloses (Xylan from corncob) and lignin aqueous solution under 300 W Xe lamp irradiation.

Figure S22. Photographs of wheat straw, corncob, polar wood chip, bamboo, rice hull, corn straw and rice straw.

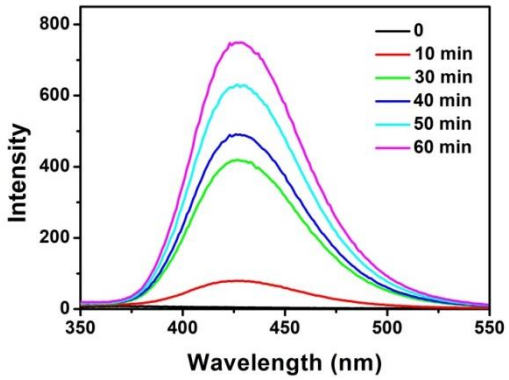

Figure S23. PL spectrum of TAOH collected from the photocatalytic system in the presence of 3% MoS_2-NGC/TiO_2 after different irradiation time.

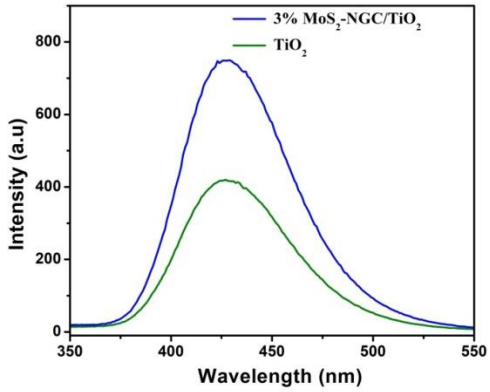

Figure S24. Comparison of PL spectrum of TAOH collected from the photocatalytic system in the presence of bare TiO_2 and 3% MoS_2-NGC/TiO_2 after 1 h of irradiation.

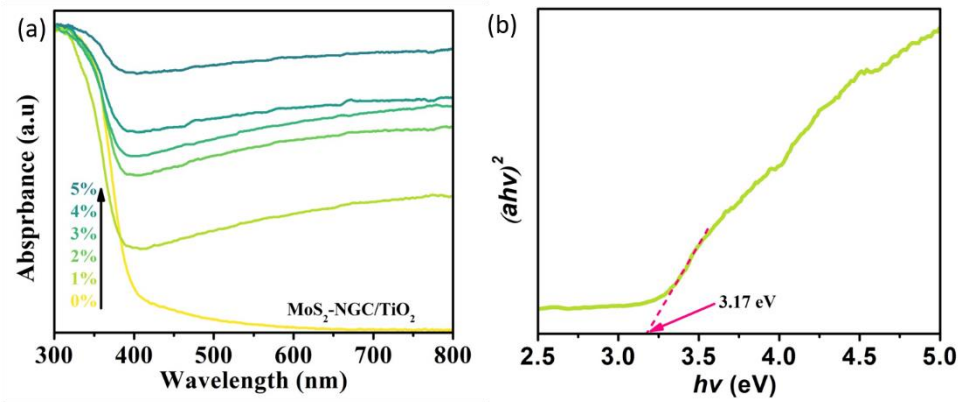

Figure S25. (a) UV-Vis spectra of MoS_2-NGC/TiO_2 photocatalysts loaded with various amount of MoS_2-NGC. (b) Bandgap of TiO_2 estimated by a related curve of $(\alpha hv)^2$ versus photon energy.

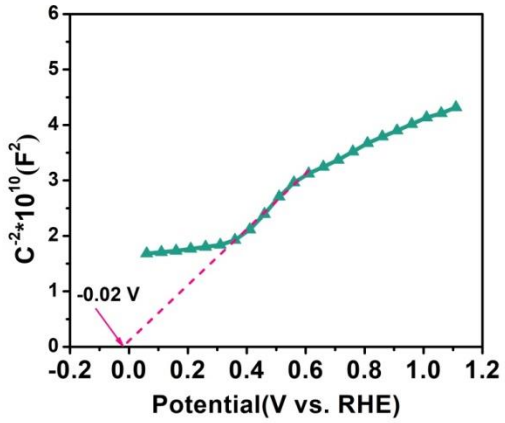

Figure S26. Mott-Schottky plots of TiO_2 electrode measured in Na_2SO_4 aqueous solution. The flat band potential of TiO_2 was observed to be approximately -0.02 V vs. RHE, and thus the CB level was located at -0.22 V vs. RHE since the CB level position was more negative 0.2 eV than its flat band potential. The VB position of TiO_2 was estimated to +2.95 V vs. RHE because the bandgap of TiO_2 was observed to be 3.17 eV (Figure S21).

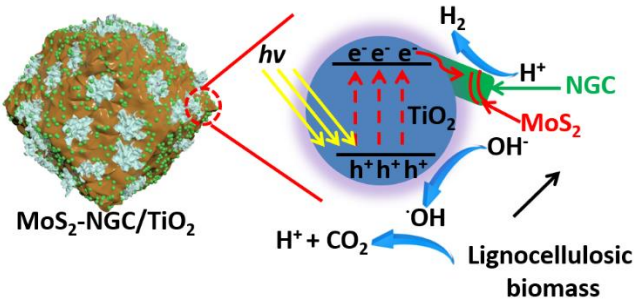

Figure S27. Proposed mechanism for photocatalytic photocataytic H_2 production from lignocellulosic biomass over MoS_2-NGC/TiO_2 photocatalysts.